Determination of moisture diffusivities in gypsum renders

O.C.G. Adan
TNO Building and Construction Research

It is generally recognised that the water transport in monolithic porous materials can be described using a macroscopic diffusion-type equation. Until now, the determination of the diffusion coefficients in this equation was a major problem. Two new non-destructive measuring techniques based on neutron beam attenuation and nuclear magnetic resonance, respectively, were applied to determine the isothermal moisture diffusivity directly from transient moisture content profiles. The experiments concerned a gypsum render.
For the first time, moisture content profiles in a dry material responding to transient relative humidities below saturation could be measured. The results show that the moisture diffusivity to be used in the modelling of moisture transfer strongly depends on the initial conditions of the material, underlining the complex interaction of liquid and vapour phases in the porous system. The moisture diffusivity for drying of the wet gypsum may exceed the moisture diffusivity of the dry gypsum exposed to transient RH's by a factor of 100. As a consequence, the experimental results refute the common estimations of hygroscopicity effects on the basis of the apparent diffusivity derived from the sorption isotherm and the water vapour permeability.

Keywords: **moisture transport, diffusivity, nuclear magnetic resonance, neutron radiography, hysteresis, gypsum.**

1 Introduction

Moisture plays a pivotal role in the deterioration of building materials. In the indoor environment, moisture problems can arise from rain penetration of the building envelope, rising damp or leakage of water supply and drainage systems. Causes of most of these problems can be related to faults in design or improper maintenance. More commonly, the origin of material dampness causing biodeterioration in the indoor environment is water vapour, most of it being generated by the normal domestic activities of the occupants.
Generally, a comprehensive understanding of the moisture transport is required to deal with problems of durability. In particular, the moisture transport at low moisture contents in the hygroscopic regime is of interest to biodeterioration problems, e.g. fungal growth. Although fungal defacement of finishing materials is often related to surface condensation, experimental evidence shows that virtually all indoor fungi optimally grow at relative humidities below saturation. Under transient conditions, the so-called time-of-wetness (Adan, 1994) appears to be a measure of the risk for microbial growth.

It is generally recognised that the macroscopic moisture transport in monolithic porous materials can be described using a non-linear diffusion-type equation. In such a model, all mechanisms for moisture transport, i.e. liquid flow and vapour diffusion with associated enhancement mechanisms, are assimilated into a single moisture diffusivity being dependent on the actual moisture content. The basic equations for combined heat and moisture transfer were first established by Philip and de Vries (1957). During past decades, the work of Whitaker (1977) and Bear and Bachmat (1990) provided a more fundamental basis for their equations.
Until now, the determination of the moisture diffusivities was a major problem. In the present study, however, two new non-destructive measuring techniques were applied to determine the moisture diffusivity directly from transient moisture content profiles in the material. The study concerns the isothermal transport in a gypsum render that is commonly found in Dutch residential buildings. The material is subjected to drying, absorption and transient relative humidities. In the case of hygroscopic response to transient relative humidities, the actual diffusivity resulting from the measurements is compared to the apparent diffusivity, estimated on the basis of the sorption isotherm and water vapour permeability.

2 Theory for moisture transport in porous media

The unidimensional and isothermal moisture transport in porous media can be approximated by a non-linear diffusion equation

$$\frac{\partial \theta}{\partial t} = \frac{\partial}{\partial x}\left(D_\theta \frac{\partial \theta}{\partial x} \right) \qquad \text{(I)}$$

In this diffusion model, all mechanisms for moisture transport are assimilated into a single moisture diffusivity D_θ, being dependent on the actual moisture content θ.
This equation represents a macroscopic model, applicable to rigid systems. Actually, the macroscopic quantities are derived by volume averaging the various transport equations on the microscopic level, i.e. within the pore geometry (Whitaker, 1977; Bear and Bachmat, 1990). These macroscopic quantities are continuous and measurable. The diffusion coefficient D_θ is related to the geometrical properties of the material, but also depends on the physical properties of water.
In this model, the effects of gravity and external pressures are neglected. Furthermore, hysteresis is still not satisfactorily implemented in the theory. As a consequence of hysteresis, the transport coefficients become a multivalued function of the moisture content, the actual value depending on the history of the previous values of the moisture content.

3 Methods

3.1 *Microcalorimetry*

Determination of sorption isotherms was performed on the basis of a microcalorimetric method, originally introduced by Van Bokhoven (1979, 1985).

The principle is schematically presented in Fig. 1. An evaporation vessel (E), containing the liquid adsorptive (l), an adsorption vessel (A) with the adsorbent (a) and a connecting tube including a valve with adjustable restriction (V_r) form a closed thermodynamic system. Heat exchange takes place only through two identical thermopiles, acting as heat flow meters. The cold junctions of both piles are connected to the constant temperature heat sink (Tc) of the calorimeter, whereas the other junctions are in contact with the vessels. Compensation for spurious heat flows due to uncontrolled temperature fluctuations is obtained by coupling two reference cells with similar thermopiles in electrically opposite sense.

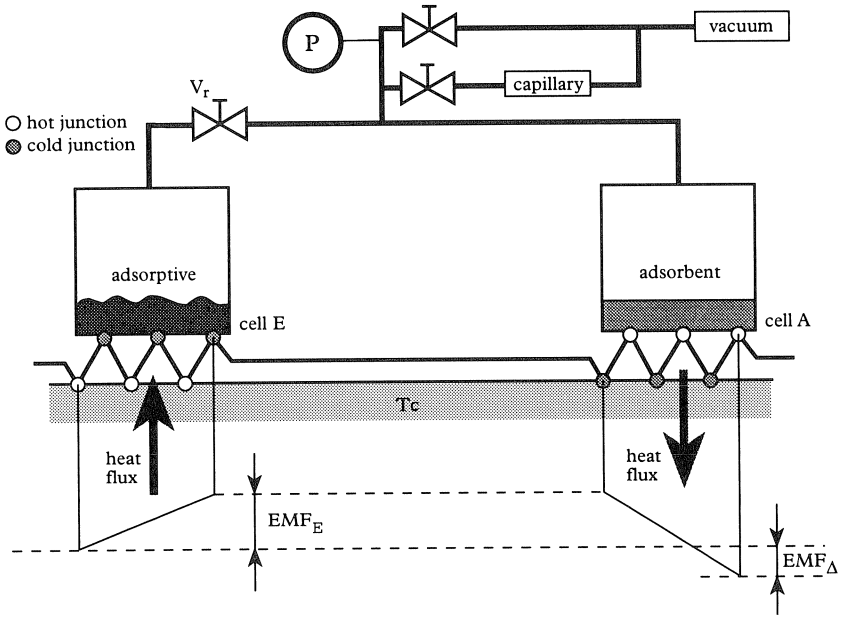

Fig. 1. Schematic presentation of the sorption microcalorimeter.
Legend: E = evaporation vessel, containing the liquid adsorptive; A = adsorption vessel containing the adsorbent; V_r = adjustable restriction; P = pressure gauge; Tc = constant temperature heat sink.

After evacuation of air and thermal equilibration of the system, the restriction V_r is opened, admitting diffusion of adsorptive to the adsorbent. Consequently, two simultaneous heat flows are introduced caused by evaporation in cell E and adsorption in cell A, respectively. These heat flows evoke two opposite electro motive forces (e.m.f.'s) in the correspondent thermopiles. Integration of the

evaporation-side e.m.f. (EMF_E) over the time interval needed for re-equilibration represents a measure of the amount of adsorptive that has been evaporated; taking the dead volume and the systems adsorption (to surfaces of cells and tubes) into account, the amount adsorbed is deduced as well. A pressure gauge (P) connected to the adsorption vessel measures the actual adsorptive vapour pressure (inaccuracy $\Delta p/p$s <1%) that is required for deduction of the adsorption isotherm. For desorption measurements, valve V_r is closed; connecting the adsorbent cell via a capillary tube to vacuum induces a vapour outflow. Vacuum is obtained from a combined rotary diffusion pumping system. From the flow characteristics of the capillary and the actual pressure difference the amount desorbed is deduced.
For description of thermodynamic equilibria, the measuring device allows simultaneous measurement of net differential heats of adsorption in addition.

3.2 *Scanning Neutron Radiography*

Because neutrons interact with atom nuclei, a neutron beam will be attenuated during transmission through a material. This interaction depends on the chemical element and is a result of scattering and absorption of the neutrons by the nucleus. The scattering by hydrogen nuclei predominates the neutron beam attenuation. Because of this sensitivity, a neutron scattering technique is very appropriate for water content determination.

For a rigid non-shrinking material, consisting of a material and a water component, the attenuation of the neutron beam intensity I_0 after transmission is obtained from

$$I = I_0 \cdot e^{-d \cdot (\mu_{mat} + \mu_w \cdot \theta)} \qquad \text{(II)}$$

where d is the equivalent thickness, μ_{mat} and μ_w are the macroscopic attenuation coefficients of the material and water, respectively. For the considered gypsum plaster, the average value of μ apeared to be 0.58 cm^{-1}, for water 2.54 cm^{-1}.

The experiments discussed in the present study were performed at the 2 MW swimming-pool type nuclear reactor of the Interfacultair Reactor Instituut, Delft University of Technology in the Netherlands. In all experiments, a monochromatic beam of thermal neutrons with a wavelength of 1.31 Å (corresponding to a 47.7 meV energy) was used, which was selected by means of a (002) reflection at a zinc crystal (Fig. 2). Application of an adjustable collimator made of boron and cadmium produced a narrow neutron beam and a high spatial resolution. A second collimator, identical to the first, was introduced in front of the detector to correct for beam divergence and multiple scattered neutrons. After transmission, neutrons were detected by a ^3He proportional detector, which has a very high detection efficiency for thermal neutrons, and a low detection efficiency for gamma rays, respectively.
Since the reactor activity may vary during the experiments, the initial beam intensity I_0 or the number of neutrons passing per unit of time may also change. Consequently, I_0 should be determined continuously. This problem has been solved by relating the detection time and thus the

number of neutrons after transmission to a fixed number of neutrons before transmission as registered by the beam monitor.
To obtain moisture content profiles, the sample is gradually moved through the beam using an elevator with a 0.02 mm positioning accuracy. The operational procedures included arrangements to eliminate mechanical hysteresis effects.

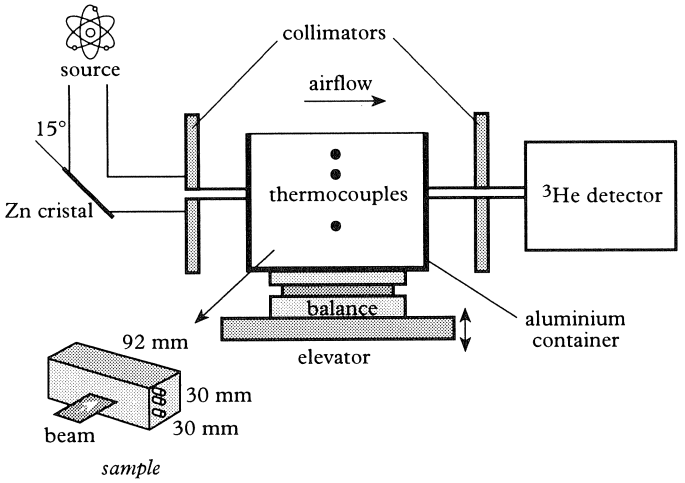

Fig. 2. Schematic presentation of the arrangement for measuring moisture content profiles in the drying experiments using scanning neutron radiography. The inset shows the sample and beam dimensions.

3.3 *Nuclear Magnetic Resonance*

Because of their rotational spin, hydrogen nuclei possess a magnetic moment. In nuclear magnetic resonance (NMR) experiments, appropriate radio frequency fields manipulate the magnetic moments of hydrogen nuclei, resulting in a so-called spin echo signal. The amplitude of this signal is proportional to the number of nuclei responding. NMR is a magnetic resonance technique where the resonance condition for the nuclei is given by

$$f = \gamma \cdot B_0 \qquad \text{(III)}$$

where f is the frequency of the radio frequency field, γ is the gyromagnetic ratio (42.58 MHz/T for ^{1}H) and B_0 is the external applied static magnetic field. Because of this resonance conditions, the method can be applied to trace hydrogen, and consequently to determine the water content. Introduction of a magnetic field gradient causes the resonance conditions to be spatially dependent. As a consequence, the moisture content distribution can be measured without moving the sample under consideration. The experiments in the present study were performed using a prototype NMR apparatus developed by Kopinga and Pel (1994).

4 Results

4.1 *Sorption isotherms and net differential heat of adsorption*

The sorption isotherm was determined for an initially dry gypsum sample, exposed to a repeated adsorption-desorption cycle between 0 and 97% relative humidity at 20 °C. The resulting water vapour isotherm (Fig. 3) shows a considerable hysteresis, extending over the whole range of *RH*'s, and some adsorbate retaining after each cycle. Generally, this sorption isotherm may be identified as type III according to the Brunauer classification (Brunauer *et al.*, 1940). Such isotherms are characteristic of weak gas-solid interactions for non porous or macroporous solids.

In Fig. 4, the net differential heat of sorption is plotted for the first adsorption and desorption cycle. For RH's above 30%, the heat of sorption exceeds the heat of liquefaction significantly in both the adsorption and desorption branch, indicating that water sorption in the second and higher adsorbed layers is not equivalent with condensation and evaporation of pure liquid water.

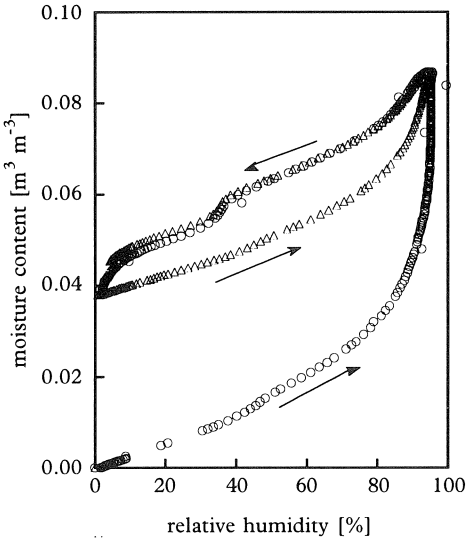

Fig. 3. (left) The water vapour isotherm of the gypsum plaster. Both the first (○) and second (Δ) traverse are shown.

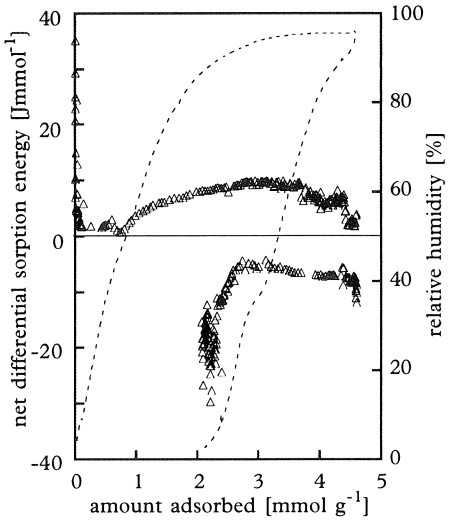

Fig. 4. (right) The net differential heat of sorption (Δ, the left y-axis) for the first sorption cycle of the gypsum plaster. The dotted line (the right y-axis) represents the corresponding traverse of the sorption isotherm.

The most plausible explanation of the large low-pressure hysteresis in the first cycle appears to be the completion of the hydration. During the hydration reaction, a net heat of 13 kJ · mol^{-1} bound water should be released. If the large hysteresis observed is due to completion of the reaction, integration of the net heat of sorption in Fig. 4 over the adsorption and desorption branches should correspond with the cumulative energy of formation of structurally bound water. Taking the

inaccuracy into account, the net energy resulting from integration ranges between 16 and 25 $J \cdot g^{-1}$ material. If the remaining adsorbate after desorption should be structurally bound, the net energy should be approximately 27 $J \cdot g^{-1}$ material.

Consequently, additional 1-day exposure to 97% RH and subsequent drying was added to the standard conditioning procedure of the gypsum samples in the experiments in the next paragraph.

It should be noted that recrystallisation, causing changes in the geometric structure with possible effects on sorption, may occur as a consequence of exposure of the gypsum to water. However, according to Lelong (1977) such effects are extremely slow, so they are neglected in the present experiments.

4.2 *Moisture content profiles and diffusivities*

Determination of the moisture diffusivity from moisture content profiles requires a fine grid of measuring points. Pel *et al.* (1993) showed that a distance of 0.5 mm between the points results in an accurate diffusivity near the minimum value at low moisture contents. For higher moisture contents, distances of some mm are sufficient. In the NMR experiments an equidistant grid of 0.15 mm was applied. Since the scanning neutron radiography is considerably slower, a variable grid was used ranging from 0.5 mm to 2 mm in the drying experiments, and 0.1 mm to 2 mm in the transient *RH* experiments, respectively. The grid size decreased on approaching the surface, where the steepest gradients in moisture content are expected.
The data set of a single scan of the material cross section consists of moisture contents on different moments in time. The profile of moisture contents on the same moment in time is deduced from cubic spline interpolation of the time dependent data of each measuring point.

4.2.1 Absorption

The base of a cylindrical sample of 20 mm diameter and a length of 80 mm was contacted with a water surface, consequently introducing free absorption. The moisture content profiles were measured using NMR. The measuring time for a single moisture content with a 2% inaccuracy was about 10 s. Each experiment lasted 2 h.
If the Boltzmann transformation $\lambda = x \cdot t^{-0.5}$ is applied, equation (I) reduces to the ordinary differential equation

$$2\frac{d}{d\lambda}\left(D_\theta \frac{d\theta}{d\lambda}\right) + \lambda\frac{d\theta}{d\lambda} = 0 \qquad \text{(IV)}$$

With the boundary conditions $\theta = \theta_s$ for $\lambda = 0$, where θ_s is the saturated moisture content under atmospheric conditions, and $\theta = 0$ as $\lambda \rightarrow \infty$, this equation has only one solution. Fig. 5 shows the Boltzman transformation of the measured moisture content profiles during absorption, yielding coinciding curves. This indicates that indeed the moisture transport during absorption can be described using a diffusion equation, and expresses the √time-relationship of the water front progression.

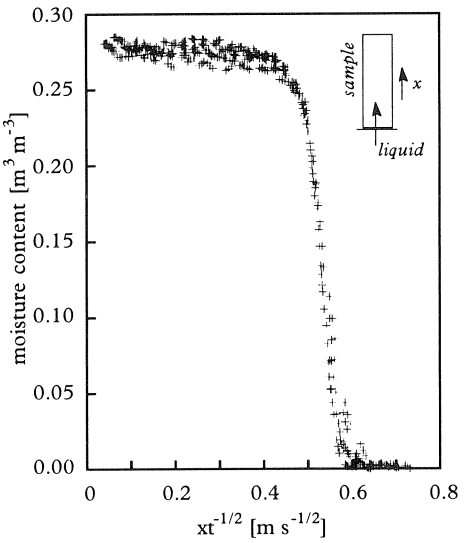

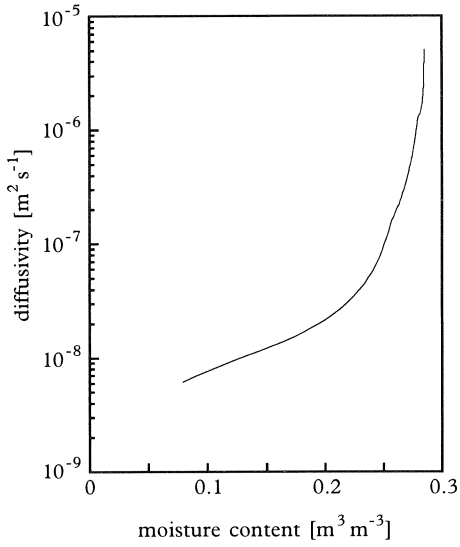

Fig. 5. (left) Boltzmann transformation of the moisture content profiles (NMR) during absorption.

Fig. 6. (right) The moisture diffusivity as deduced from the moisture content profiles in the absorption experiments.

From the transformed set of data, the moisture diffusivity for water absorption can be deduced by integration of equation (IV) to λ:

$$D_\theta = -\tfrac{1}{2} \cdot \frac{1}{\left(\frac{d\theta}{d\lambda}\right)_\theta} \cdot \int_{\theta_0}^{\theta} \lambda d\theta \qquad \text{(V)}$$

The resulting diffusivity as related to the moisture content is given in Fig. 6.

4.2.2 Drying

The gypsum sample of 25 × Ø20 mm^3 was immersed in demineralised water for several min. The sample was placed in a holder, open on the top side only. Exposure of this side to an air flow of 40% *RH* parallel to the surface created a unidimensional drying experiment. The experiments for each sample took 24 to 48 h.

The NMR-results for the gypsum render are given in Fig. 7. Measuring a single profile with an inaccuracy of 1% and a 0.15 mm grid typically takes about 40 min. The variations in the moisture content profiles reflect the inhomogeneities in the sample. The figure clearly shows a receding front entering the material. From this moment, the drying is internally limited by vapour transfer causing a distinct decrease both in the drying rate and the heat extracted for drying, and the experiment may be considered isothermal (Pel *et al.*, 1993). This was checked by independent temperature measurements in the same experimental arrangement.

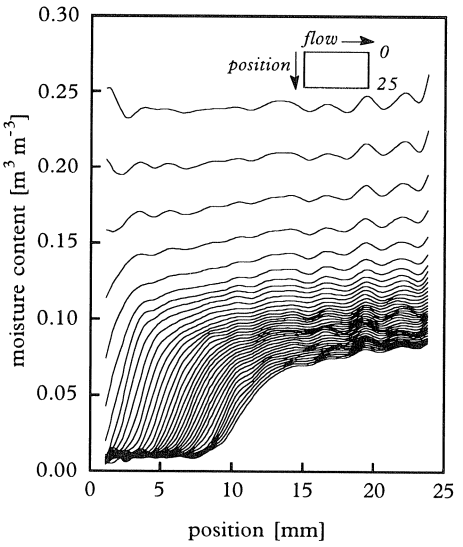

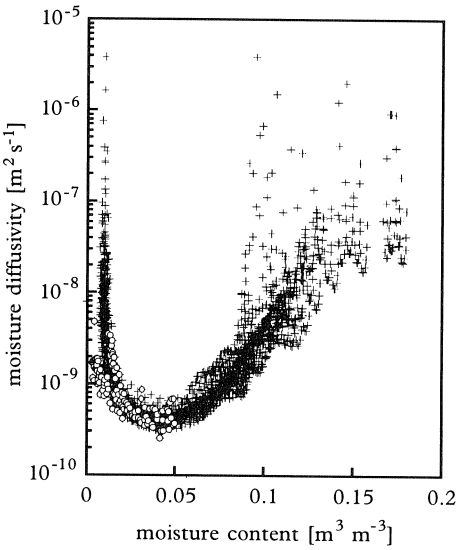

Fig. 7. (left) Moisture content profiles (NMR) during drying of the gypsum plaster. Each line represents the moisture content profile in the material at a given point of time.The time between subsequent profiles is 40 min.

Fig. 8. (right) The moisture diffusivity as deduced from measured moisture content profiles during drying of the gypsum plaster. (+) Results from NMR; (○) results from scanning neutron radiography.

For the isothermal unidimensional drying, the diffusivity can be deduced from the moisture content profiles by integrating equation (I) to x. Since the partial derivative of the moisture content with respect to the place is zero at the vapour tight bottom (x = l), this equation reads

$$D_\theta = \frac{\int_l^x \frac{\partial \theta}{\partial t}\, dx}{\left(\frac{\partial \theta}{\partial x}\right)_x} \qquad \text{(VI)}$$

The moisture diffusivity resulting from the transient moisture content profiles is given in Fig. 8. The minimum in the diffusivity at 0.04 m^{3}m^{-3} corresponds to the occurrence of a receding drying front; for lower moisture contents the vapour transport is predominant and defines the drying rate, whereas for higher moisture contents the liquid transport becomes increasingly important. Fig. 8 also includes the moisture diffusivity in the low moisture content region, resulting from the scanning neutron radiography of the same material. On comparison with the NMR results there appears to be hardly any difference.

4.2.3 Transient relative humidities

A dry gypsum sample of 76 × 30 × 5 mm was exposed to alternating levels of the relative humidity (*RH*). The *RH*'s were defined using saturated aqueous salt solutions in two containers. Each

container was part of a separate main system with a permanent circulation of air, driven by a small fan. Both systems were equipped with a by-pass, connecting the sample container to the main systems. By means of pneumatic valves, controlled by time switches, the *RH* and the corresponding system were selected. The *RH* was monitored in the air flow before and after passing the sample surface, as well as in the containers of the aqueous salt solutions. In the present experiments, *RH* above the sample surface varied between 5% and 95%.

The moisture content profiles in the gypsum were determined using scanning neutron radiography only. Since only a small layer of some mm of the material is involved in the hygroscopic response, a narrow neutron beam was used, giving a spatial resolution of 0.2 mm. The time needed for a single scan of the material was 30 min, with a measuring time of 100 s for each measuring point. During the experiments, the mean ambient temperature was 20 °C, with a maximum daily deviation of 1°C.

A typical example of the moisture content profiles in the surface layer is shown in Fig. 9.
Obviously, some water is retained after the first high RH exposure, corresponding to the moisture content at 5% *RH* on the desorption branch of the sorption isotherm of the fully hydrated material (Fig.11). Similar to the drying experiments, the moisture diffusivity is calculated from the moisture content profiles on the basis of expression (VI). Fig. 10 shows the results of repeated experiments of different samples.

The isothermal vapour diffusivity $D_{\theta v}$ can also be *estimated* on the basis of the sorption isotherm and the water vapour permeability δ according to

$$D_{\theta V} = \delta \frac{p_s}{\rho_l} \left(\frac{\partial RH}{\partial \theta} \right)_r \qquad \text{(VII)}$$

The water vapour permeability of gypsum was determined on the basis of the common wet cup-dry cup method. In Table 1, the results are given as a function of the *RH*'s on opposite sides of the gypsum sample under consideration.
The consequent estimation of the moisture diffusivity is plotted in Fig. 10 by the dotted line. As with the moisture diffusivity from the moisture content profiles, the value decreases with increasing moisture contents.

Table 1. The water vapour permeability of the gypsum render as a function of the *RH*'s on opposite sides of the sample under test.

RH on opposite sides [%]	Water vapour permeability [10^{-11} s]
53->43	2.2
65->53	2.9
75->65	3.8
85->75	3.2
93->85	4.1
97->93	4.5

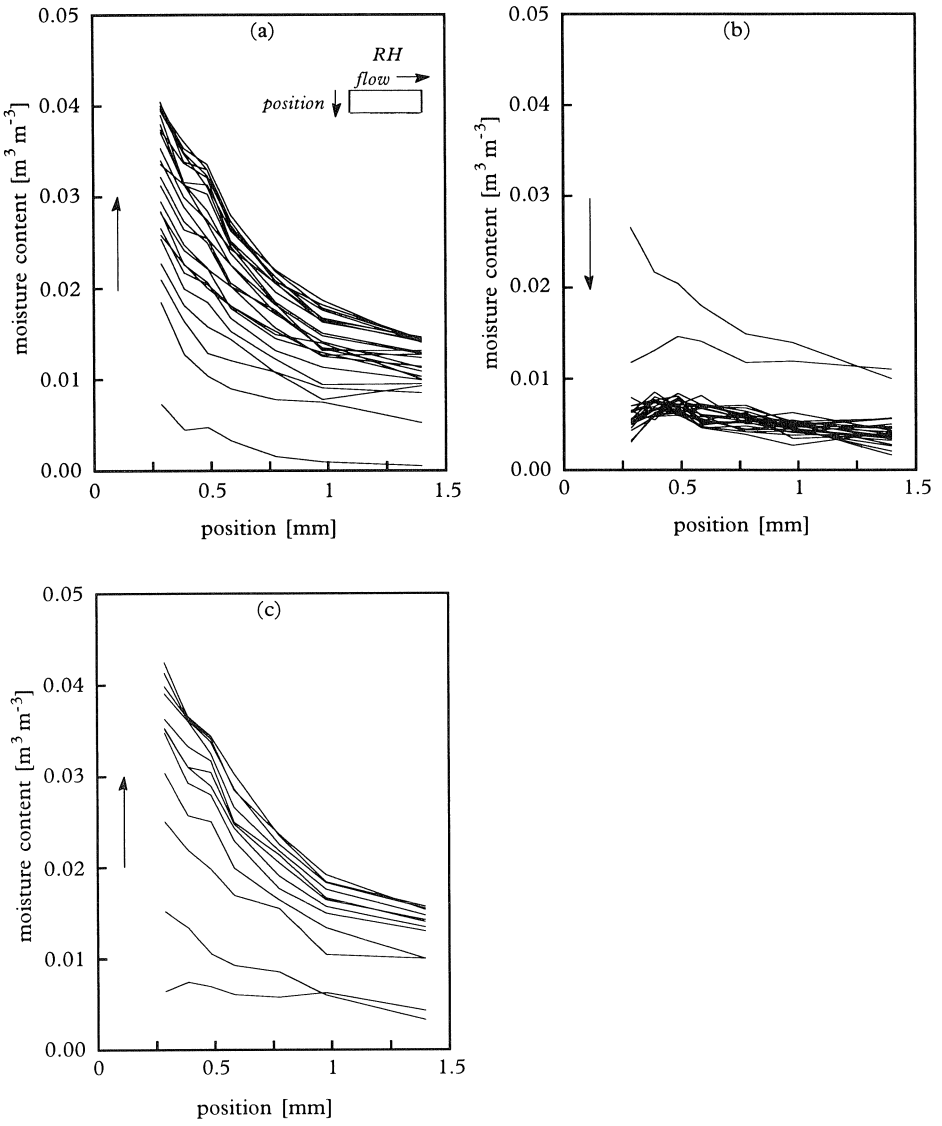

Fig. 9. Moisture content profiles as measured in the transient RH experiments using scanning neutron radiography. Each line represents the moisture content profile in the material at a given point of time. The time between subsequent profiles is 30 min.
(a) Response to the first increase in RH; (b) response to the first decrease in RH; (c) response to the second increase in RH.

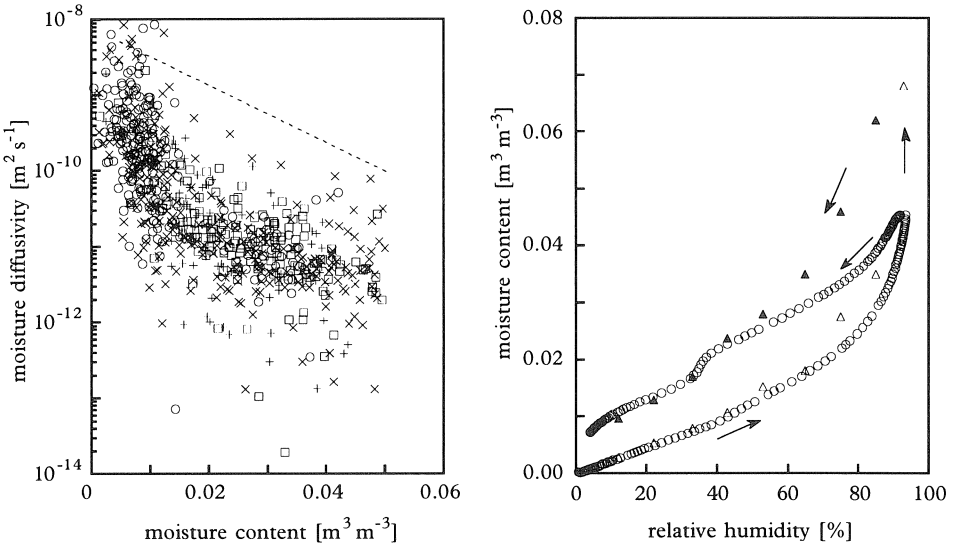

Fig. 10. The moisture diffusivity as deduced from the moisture content profiles during transient RH's. The dotted line represents the estimated diffusivity on the basis of the sorption isotherm (Fig. 11) and the water vapour permeability.

Fig. 11. The sorption isotherm (T = 20 °C) of the gypsum plaster after progressed completion of the hydration reaction, as measured with the microcalorimetric method. A second hysteresis loop is determined gravimetrically and shows (Δ) adsorption of the dry material and (▲) desorption of the same material that was initially immersed in water.

5 Discussion and conclusions

In Fig. 12, the calculated diffusivities from the experiments are schematically presented in three curves. For high moisture contents, i.e. the region where liquid transfer dominates, the diffusivities from the absorption and drying experiments seem to ally closely. The diffusivity of the drying experiments exhibits a minimum at a moisture content of approximately 0.04 m^3m^{-3}, corresponding to the introduction of a receding drying front. In this region of low water contents, the NMR and scanning neutron radiography yielded coinciding diffusivities.

For the first time, water content profiles in a dry material responding to transient relative humidities could be measured. The diffusivity deduced on the basis of these experimental data and the *estimation* on the basis of the water vapour permeability and sorption isotherm, however, deviate considerably from the diffusivity in the same moisture content regime in the drying experiments. Differences of the order of 100 occur, implying that the drying rate of a material at a given moisture content is strongly dependent on the initial state.
Several explanations can be found in the literature for the substantial differences between the *estimated* vapour diffusivity and the diffusivity from the drying experiments. In their original work,

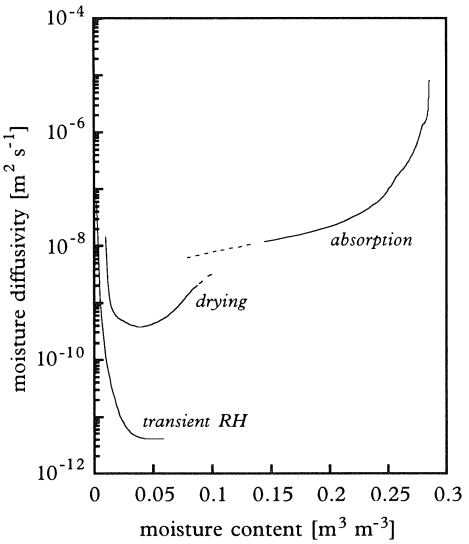

Fig. 12. Stylised picture of the moisture diffusivity from the moisture content profiles, as related to the experimental conditions.

Philip and de Vries pointed out that the simple theory of water vapour diffusion in porous media neglected the interaction of vapour, liquid and solid phases, enhancing the vapour transport.

In the present transient RH experiments, no substantial capillary condensation will occur, since 98% of the gypsum pore volume concerns pore sizes> 10^{-7} m (Adan, 1994). Consequently, no significant enhancement of the vapour flow due to the presence of liquid islands will occur during the experiments considered. However, starting from an initially wet material, a substantial part of the pores with sizes>10^{-7} m will contain liquid islands due to hysteresis. This is also indicated in the sorption isotherm in Fig. 11. Probably these effects explain the considerable differences in the moisture diffusivities at moisture contents in the high RH range.
The present experimental results clearly show that the effects of hysteresis are reflected in seperate moisture diffusivities corresponding to each initial condition of the material.
Furthermore, as a consequence of the low value of the moisture diffusivity from the transient *RH* experiments, no hygroscopic inertia effects of the gypsum render will occur in the indoor environment. In this case, the experimental results refute common estimations of hygroscopic effects on the basis of the apparant diffusivity derived from the sorption isotherm and water vapour permeability. Using the estimated diffusivity results in overestimated penetration depths, corresponding to considerable deviations in the moisture flow (Adan, 1994).

Acknowledgements

The author is indebted to dr. ir. L. Pel (Eindhoven University of Technology) for his essential contribution to the experiments, to prof. dr. ir. K. Kopinga (Eindhoven University of Technology) for the application of the prototype NMR apparatus, and to dr. J.J.G.M. van Bokhoven (TNO Prins Maurits Laboratory) for his contribution to the microcalorimetric measurements. The author also wish to thank dr. ir. A.A. van Well and ing. P. van der Ende (Interfacultair Reactor Instituut) for their indispensable help in the neutron radiography experiments, A.W.B. Theuws and H. Smulders in building and operating the experimental arrangements, and ir. H.J.P. Brocken for his assistance in the analyses.

Notations

B	(external applied) magnetic field strength [T]
D_θ	isothermal moisture diffusivity [$m^2 \cdot s^{-1}$]
d	material thickness [m]
f	resonance frequency [MHz]
I	neutron beam intensity after transmission [$m^{-2} \cdot s^{-1}$]
I_0	neutron beam intensity before transmission [$m^{-2} \cdot s^{-1}$]
p	water vapour pressure[Pa]
RH	relative humidity [%]
t	time [s]
x	spatial co-ordinate [m]
δ	water vapour permeability [s]
γ	gyromagnetic ratio [MHz $\cdot$ T^{-1}]
λ	Boltzmann transform [$m \cdot s^{-0.5}$]
μ_i	macroscopic attenuation coefficient of component i [cm^{-1}]
ρ	density [$kg \cdot m^{-3}$]
θ	volumetric moisture content [$m^3 \cdot m^{-3}$]
mat	material
l	liquid water
s	saturated
v	water vapour
w	water

References

ADAN, O.C.G. (1994) *On the fungal defacement of interior finishes*, Ph.D. Thesis, Eindhoven University of Technology.

BEAR, J. and Y. BACHMAT (1990) *Introduction to modeling of transport phenomena in porous media*, Vol. 4, Kluwer, Dordrecht.

BOKHOVEN, J.J.G.M. van (1979) A method to measure the net heat of adsorption and the adsorption isotherm simultaneously, *Thermochimica Acta* **34**: 109–126.

BOKHOVEN, J.J.G.M. van (1985) Refinement of a calorimetric method of measuring heats of adsorption and a comparison with an alternative method, *Thermochimica Acta* 86: 257–271.

BRUNAUER, S., DEMING, L.S., DEMING, W.E. and E. TELLER (1940) On a theory of the van der Waals adsorption of gases, *J. Am. Chem. Soc.* **62**: 1723–1732.

KOPINGA, K. and L. PEL (1994) One dimensional scanning of moisture in porous materials with NMR, *Rev. Sci. Instrum.* **65**: 3673–3681.

LELONG, B. (1977) Effets a long terme de l' influence de l' eau liquide sur les proprietes des platres pris, in: *Sulfates de calcium et matériaux derivés* (eds. M. Murat and M. Foucault), pp. 371–382, Compte-Rendu du Colloque Inter-national de la RILEM, Saint-Remy-Les-Chevreuse.

PEL, L., A.A.J. KETELAARS, O.C.G. ADAN and A.A. VAN WELL (1993) Determination of moisture diffusivity in porous media using scanning neutron radiography, *Int. J. Heat Mass Transfer* **36**:1261–1267.

PHILIP, J.R. and D.A. DE VRIES (1957) Moisture Movement in Porous Materials under Temperature Gradients, *Trans. Amer. Geophys. Union* **38**: 222–232.

WITHAKER, S. (1977) Simultaneous heat, mass and momentum transfer in porous media. A theory of drying porous media, *Adv. Heat Transfer* **13**: 119–200.